

Whole Exome Sequencing Reveals the Order of Genetic Changes during Malignant Transformation and Metastasis in a Single Patient with NF1-plexiform Neurofibroma

Angela C. Hirbe¹, Sonika Dahiya², Christopher A. Miller³, Tiandao Li³, Robert S. Fulton³, Xiaochun Zhang², Sandra McDonald², Katherine DeSchryver², Eric J. Duncavage², Jessica Walrath^{4,5}, Karlyne M. Reilly^{4,5}, Haley J. Abel⁶, Melike Pekmezci⁷, Arie Perry^{7,8}, Timothy J. Ley³, and David H. Gutmann⁸

Abstract

Purpose: Malignant peripheral nerve sheath tumors (MPNST) occur at increased frequency in individuals with neurofibromatosis type 1 (NF1), where they likely arise from benign plexiform neurofibroma precursors. While previous studies have used a variety of discovery approaches to discover genes associated with MPNST pathogenesis, it is currently unclear what molecular events are associated with the evolution of MPNST from plexiform neurofibroma.

Experimental Design: Whole-exome sequencing was performed on biopsy materials representing plexiform neurofibroma ($n = 3$), MPNST, and metastasis from a single individual with NF1 over a 14-year period. Additional validation cases were used to assess candidate genes involved in malignant progression, while a murine MPNST model was used for functional analysis.

Results: There was an increasing proportion of cells with a somatic *NF1* gene mutation as the tumors progressed from

benign to malignant, suggesting a clonal process in MPNST development. Copy number variations, including loss of one copy of the *TP53* gene, were identified in the primary tumor and the metastatic lesion, but not in benign precursor lesions. A limited number of genes with nonsynonymous somatic mutations (β_{III} -spectrin and ZNF208) were discovered, several of which were validated in additional primary and metastatic MPNST samples. Finally, increased β_{III} -spectrin expression was observed in the majority of MPNSTs, and shRNA-mediated knockdown reduced murine MPNST growth *in vivo*.

Conclusions: Collectively, the ability to track the molecular evolution of MPNST in a single individual with NF1 offers new insights into the sequence of genetic events important for disease pathogenesis and progression for future mechanistic study. *Clin Cancer Res*; 21(18); 4201–11. ©2015 AACR.

Introduction

Neurofibromatosis type 1 (NF1) is one of the most common tumor predisposition syndromes, affecting as many as 1 in 2,500 people worldwide (1). Similar to other tumor predisposition syndromes, patients with NF1 are born with a germline mutation in one copy of the *NF1* gene. Tumors arise following somatic loss of the other *NF1* allele in the appropriate cell of

origin. Among the tumor types most frequently encountered in this inherited cancer syndrome are benign and malignant tumors involving the peripheral nervous system, including benign dermal neurofibromas, benign plexiform neurofibromas, and malignant peripheral nerve sheath tumors (MPNST). Dermal neurofibromas are observed in nearly all adults with NF1, while plexiform neurofibromas and MPNSTs are found in 33% to 50% and 10% to 13% of individuals with NF1, respectively (2, 3). In contrast with dermal neurofibromas, which do not progress to cancer, plexiform neurofibromas can transform into MPNSTs (2).

MPNSTs represent an aggressive type of Schwann cell-derived neoplasm associated with poor overall patient survival. Currently, there are limited therapeutic options, and survival remains dismal following surgical removal, radiation therapy, and chemotherapy. Moreover, there are few clinicopathological factors that influence outcome, and no accurate biologic markers for disease progression. In contrast with other soft tissue sarcomas, there are no pathognomonic chromosomal translocations, and conventional cytogenetic analyses typically demonstrate complex karyotypes in MPNSTs.

In NF1-associated MPNST, bi-allelic inactivation of the *NF1* gene has been reported in approximately 60% to 90% of tumors (4–6), whereas loss of *NF1* protein (neurofibromin) expression is seen in nearly 90% of NF1-associated cases (7). Similarly,

¹Division of Medical Oncology, Department of Medicine, Washington University School of Medicine, St. Louis, Missouri. ²Department of Pathology and Immunology, Washington University School of Medicine, St. Louis, Missouri. ³Department of Genetics, The Genome Institute at Washington University, St. Louis, Missouri. ⁴Rare Tumors Initiative, National Cancer Institute, Bethesda, Maryland. ⁵Division of Statistical Genomics, St. Louis, Missouri. ⁶Department of Pathology and ⁷Neurological Surgery, UCSF School of Medicine, San Francisco, California. ⁸Department of Neurology, Washington University, St. Louis, Missouri.

Note: Supplementary data for this article are available at Clinical Cancer Research Online (<http://clincancerres.aacrjournals.org/>).

Corresponding Author: David H. Gutmann, Washington University School of Medicine, 660 S. Euclid Avenue, Campus Box 8111, St. Louis, MO 63110. Phone: 314-362-7379; Fax: 314-362-2388; E-mail: gutmann@neuro.wustl.edu

doi: 10.1158/1078-0432.CCR-14-3049

©2015 American Association for Cancer Research.

Translational Relevance

Currently, the molecular pathogenesis of malignant peripheral nerve sheath tumors (MPNST) is incompletely understood due to the rarity of these tumors. Because treatment options are limited and no efficacious biologically targeted therapies are presently available, there is a pressing need to better define the genetic events critical for MPNST development and progression. Herein, we leveraged whole-exome sequencing to genomically define the progression of tumor development from benign precursor lesions to malignant and metastatic MPNST in a single patient with NF1. Several candidate genes were revealed and subsequently validated in an independent series of MPNSTs, including *SPTBN2* and *ZNF208*. In addition to mutations in the *SPTBN2* (β_{III} -spectrin) gene, we found robust β_{III} -spectrin immunoreactivity in the majority of MPNSTs, but not in their benign counterparts. Moreover, β_{III} -spectrin knockout reduces murine MPNST growth *in vivo*, thus identifying a new potential candidate gene for further mechanistic study.

approximately 40% to 60% of sporadic MPNST harbor a somatic mutation in the *NF1* gene (5, 6, 8) and 43% have loss of neurofibromin expression (7), supporting an important role for the *NF1* tumor suppressor gene in the development of both sporadic and NF1-associated MPNSTs. Although *NF1* loss is required for MPNST development, it is not sufficient for malignant transformation. As such, genetically engineered mice with conditional *Nf1* gene inactivation in Schwann cell precursors do not develop MPNSTs (9–13): MPNST formation requires the acquisition of additional genetic mutations that cooperate with loss of *NF1* gene function to promote malignant transformation. In mouse and human tumors, alterations in the *TP53*, *CDKN2A*, and *EGFR* genes contribute to MPNST pathogenesis (14, 15). Similarly, previous studies have used a variety of discovery platforms to identify other genes critical for human plexiform neurofibroma malignant progression (14, 16–23). Unfortunately, few of these genes are common across studies, and none have emerged as accurate predictors of disease pathogenesis.

In an effort to define the genetic alterations important for malignant progression of plexiform neurofibroma to MPNST, we used whole-exome sequencing technologies. Using a single patient with NF1 with a plexiform neurofibroma followed over a 14-year period, we established the sequence of genetic events associated with malignant transformation and progression (metastasis). Additional validation cases were subsequently used to further assess candidate genes involved in malignant progression. One of these mutated genes (β_{III} -spectrin) was found to be overexpressed in the majority of MPNSTs, and its silencing dramatically attenuated murine MPNST growth *in vivo*.

Materials and Methods

Patients

Blood, tumor, and other normal tissues were obtained from individuals diagnosed with NF1 according to established criteria (24) and treated at Washington University/St. Louis Children's Hospital NF Clinical Program (St. Louis, MO) or at the University of California San Francisco (San Francisco, CA) under active

Human Studies Protocols approved by the Institutional Review Boards at each respective institution in accordance with the 1964 Helsinki Declaration and its later amendments or comparable ethical standards. Whole-exome sequencing or sequencing of target genes was performed on tumor and matched normal DNA. Tumor DNA samples were obtained from formalin-fixed paraffin-embedded (FFPE) blocks or frozen tissue (when available) obtained at surgical resection or biopsy. Normal paired DNA was isolated from peripheral blood obtained by phlebotomy or from adjacent normal tissue from paraffin-embedded blocks at surgical resection or biopsy on deceased patients for whom a peripheral blood sample could not be obtained.

Pathology review and laser capture microdissection

Images of hematoxylin and eosin-stained slides from the discovery patient and validation patients were created on an Aperio ScanScope XT. The Aurora mScope viewer was used to view the images and obtain images at $\times 20$ magnification. A pathologist (S.M. Dahiya or K. DeSchryver) assessed a digitized hematoxylin and eosin-stained slide to determine and outline tumor nests, thereby mapping the section, and directing the laser capture microdissection (LCM) to areas of irrefutably high tumor cell content on the adjacent FFPE sections. Five to 10 sections (10 μ m thick) from each FFPE block were cut on a microtome (Leica RM 2255), air dried for 2 hours or longer, and placed at 60°C for 30 minutes. The sections were stored at 4°C until use or were immediately stained with a rapid hematoxylin and eosin ethanol-based staining protocol. Within 10 minutes of air-drying, the slide was placed on the LCM stage of Arcturus PixCell instrument for microdissection. The desired cells were microdissected into the cap of 500- μ L safe-lock tubes filled with 50 μ L ALT buffer (Qiagen). This procedure was repeated on the next slide until a total of 2,000 to 5,000 cells of interest had been captured for each case. The number of (adjacent) slides used per case to reach this 2,000-cell threshold varied from 5 to 10, as tumor proportion varied across samples.

DNA extraction

LCM-derived DNA samples were isolated from 2,000 to 5,000 cells using a Qiamp DNA micro kit (Qiagen Cat. #56304) following RNase A treatment, according to the manufacturer's instructions. DNA was quantified using a NanoDrop 2000 spectrophotometer (Thermo Fisher Scientific).

Exome sequencing

DNA was fragmented using a Covaris E210 DNA Sonicator (Covaris) with a size range between 100 bp and 400 bp. Libraries were prepared using a SciClone instrument (PerkinElmer). Short (8 bp) index sequences were utilized during library construction to enable sample multiplexing. For this work, two pools were created for capture: one pool with the FFPE samples and one with fresh-frozen sample, since the capture efficiencies between FFPE and frozen libraries are not compatible. Libraries were pooled (300 ng/library) for hybrid capture and individually processed using the Roche NimbleGen V3 Design Exome reagent (Roche Nimblegen) covering approximately 64 Mb of the human genome. The libraries were hybridized for 64 to 72 hours at 47°C followed by stringent washing. Enriched ssDNA library fragments were eluted and amplified prior to sequencing. Capture products were pooled and first run across two lanes of HiSeq 2000. Because

of low cluster density on the original flow cell, an additional lane of HiSeq 2000 was also generated to achieve a minimum coverage of all targeted space, with >80% coverage at >20× coverage. Upon completion of the sequencing runs, data were processed through an automated data processing system to yield sample quality metrics as well as sequence variants relative to the human genome reference sequence.

Variant calling

Exome sequence data were aligned to the reference sequence build GRCh37-lite-build37 using bwa version 0.5.9 (ref. 25; params: -t 4 -q 5::), and then merged and duplicated using picard version 1.46 (<https://broadinstitute.github.io/picard/>). SNVs were detected using the union of three callers including: (i) Samtools version r963 (ref. 26; params: -A -B) filtered by snp-filter version v1 and intersected with Somatic Sniper version 1.0.2 (ref. 27; params: -F vcf -q 1 -Q 15) filtered by false-positive version v1 (params: -bam-readcount-version 0.4 -bam-readcount-min-base-quality 15) following by somatic-score-mapping-quality version v1 (params: -min-mapping-quality 40 -min-somatic-score 40), (ii) VarScan 2.2.6 (28) filtered by varscan-high-confidence version v1 and then false-positive version v1 (params: -bam-readcount-version 0.4 -bam-readcount-min-base-quality 15), and (iii) Strelka version 0.4.6.2 (ref. 29; params: isSkipDepthFilters = 1). Indels were detected using the union of three callers including: (i) Gatk-somatic-indel version 5336 (30) filtered by false-indel version v1 (params: -bam-readcount-version 0.4 -bam-readcount-min-base-quality 15), (ii) Pindel version 0.5 (31) filtered by pindel-somatic-calls version v1 followed by pindel-vaf-filter version v1 (params: -variant-freq-cutoff = 0.08) and pindel-read-support version v1, VarScan 2.2.6 (30) filtered by varscan-high-confidence-indel version v1 and false-indel version v1 (params: -bam-readcount-version 0.4 -bam-readcount-min-base-quality 15), and (iii) Strelka version 0.4.6.2 (ref. 29; params: isSkipDepthFilters = 1).

Data production for validation

Of note, 250 ng aliquots were generated for library construction using the KAPA HTP sample prep kit (KAPA Biosystems). DNA was fragmented using a Covaris E210 DNA Sonicator (Covaris) with a size range between 100 bp and 400 bp. Libraries were prepared using a SciClone instrument (PerkinElmer). Short (8 bp) index sequences are utilized during library construction to enable sample multiplexing. A dual index approach is utilized in which unique sample indices are placed at each end of the ligated library fragment, providing a stringent sample match condition ensuring data is associated with the appropriate sample.

Libraries were pooled at equal molar concentrations of library. A total of 5 µg of library pool was hybridized using biotinylated 120 bp biotinylated oligo nucleotides (IDT lockdown probes, Integrated DNA Technologies) specific to the genes of interest based on the discovery phase of the project. Libraries were then hybridized for 72 hours at 47°C followed by stringent washing. Enriched ssDNA library fragments were eluted and amplified prior to sequencing. DNA sequencing was performed using one lane of a flow cell of 2 × 100 bp reads on an Illumina HiSeq 2000 sequencer.

Manual review

Mapped reads were manually inspected to confirm the automated variant calls and frequency using IGV (Integrative Genomics Viewer). Review criteria required that (i) the variant was supported by at least 5% of the high-quality reads with a min-

imum of two reads supporting the variant, (ii) the variant was supported by reads in both sequencing directions, (iii) the variant base was high quality (brightly colored in display), (iv) the reads containing the variant had no more than two high-quality mismatches relative to the reference genome (excluding dnbsnps), and (v) the reads supporting the variant mapped uniquely to the reference genome. On the basis of these criteria, variants are either confirmed or denied.

Copy number analysis

Copy number variation (CNV) calls were made from the exome data using the Copy Change Assessment Tool 2 (CopyCAT2). Briefly, sequence data files (BAMs) for each case were used to calculate coverage for each bait position in the exome reagent. The resulting coverage data were normalized to a set of 12 unrelated normal control exomes sequenced to a similar coverage depth using the same capture reagent and sequencing chemistry using loess statistics. Variant allele frequencies were also calculated for SNPs within each gene. Segments of constant copy number were identified using circular binary segmentation, and confirmed by skewing of the variant allele frequencies. Data are then plotted to provide visualization of CNVs.

IHC and tissue microarray generation

IHC staining was performed using rabbit polyclonal β_{III}-spectrin antibody (H-70; Santa Cruz Biotechnology; dilution 1:200) or goat polyclonal ZNF208 antibody (Santa Cruz Biotechnology; dilution 1:50) with citrate antigen retrieval. Previously generated tissue microarray blocks contained at least two cores of tissue (2 mm in diameter) from the most representative areas of tumor as well as from normal peripheral nerve (32).

Lentiviruses

Lentiviral *Sptbn2* shRNA (sigma) or control LacZ shRNA (Genome Institute at Washington University) containing pLKO.1 plasmids was utilized for *in vitro* and *in vivo* MPNST tumor cell line growth experiments. Two Lentiviral *Sptbn2* shRNA constructs were screened, but only one construct led to decreased levels of β_{III}-spectrin as determined by Western blotting and this construct was chosen for further experiments. The FUW-FLG lentiviral vector encoding firefly luciferase and GFP was utilized to generate tumor cell lines that could be followed *in vitro* and *in vivo* by bioluminescence imaging (BLI). Viral particles were produced by the Viral Vectors Core Facility of the Hope Center for Neurological Diseases at Washington University School of Medicine. See Supplementary Table S1.

Western blotting

Cell pellets were lysed in buffer containing 1% NP-40 (non-ylphenoxypolyethoxyethanol), supplemented with protease inhibitors. Western blotting was performed as previously described (33) and according to manufacturer's instructions regarding antibody use with β_{III}-spectrin (H-70; Santa Cruz Biotechnology; dilution 1:200) and α-tubulin (Sigma; dilution 1:10000).

Murine MPNST cell lines

Murine MPNST tumor lines were established from male C57BL6/J *Nf1*^{+/-}; *Trp53*^{+/-}-cis (*NPcis*) mice that inherited the mutant allele from the father (*NPcis*-paternal; refs. 34, 35). Briefly, palpable masses were divided into two sections for (i) histologic

Hirbe et al.

analysis and (ii) cell line generation. Tumor pieces were triturated in Triple Express (Gibco) and DNase (Roche) in 24-well plates for 2 to 5 hours at 37°C in 5% CO₂, and successively passaged in DMEM with 10% FBS. Four lines were used in this study, including JW12 (10 × 5 × 8 mm jaw mass from a 153-day-old mouse), JW15 (15 × 9.5 × 8.5 mm leg mass from a 134 day-old mouse), JW18 (9.2 × 6 × 3 mm shoulder mass from a 99-day-old mouse), and JW23 (15 × 22 × 16 mm jaw mass from a 104-day-old mouse). JW18 cells were confirmed as MPNST by immunocytochemical analyses using S100 (1:1000 rabbit anti-cow; Dako), MyoD1 (1:50 mouse clone 5.8A; Dako), and Myf4 (1:30 mouse 1554; Novocastra) antibodies with appropriate secondary Alexa Fluor-499 antibodies (Invitrogen) and DAPI counterstaining. Cells were mounted in Vectashield, and photomicrographs acquired at ×40 magnification using SPOT 3.5.9 for MacOSX with a Nikon Eclipse E6000 camera. The RD cell line, derived from a human rhabdomyosarcoma (a kind gift from Javed Khan, NIH, Bethesda, MD) was used as a positive control for MyoD1 and Myf4 (Supplementary Fig. S1).

Murine MPNST cell lines were then transduced with green fluorescent protein (GFP)-luciferase viral supernatants as previously described (36, 37), and sorted by GFP expression using flow cytometry. Each cell line was plated at serial dilutions to

ensure clonal derivation. Several clones from each cell line were screened for luciferase expression. The highest expressing clone from each cell line was expanded (JW18.2, JW12.1, JW15.3, JW23.3) for use.

Bioluminescence imaging

Bioluminescence imaging (BLI) was performed on an IVIS 50 (PerkinElmer; Living Image 4.1, 1 sec–5 minutes exposures, binning 8, FOV 12 cm, *f*/stop1, open filter). *In vivo* bioluminescence was measured on days 5, 9, 12, and 16 posttumor cell injection following i.p. injection of D-luciferin (150 mg/kg; Gold Biotechnology, Inc.). For the *in vitro* assays, cells were plated in 24-well black-walled plates and imaged 24, 48, and 96 hours later, after the addition of D-luciferin (150 µg/mL). Total photon flux (photons/second) was measured from software-defined regions of interest using Living Image 2.6.

In vitro tumor growth assay

A total of 10⁵ JW18.2-sh*Sptbn2* or JW18.2-sh*Luc2* cells were plated in each of 6 wells of a 24-well plate. Cells were imaged by BLI and then manually counted at 24 hours, 48 hours, and 96 hours post-plating.

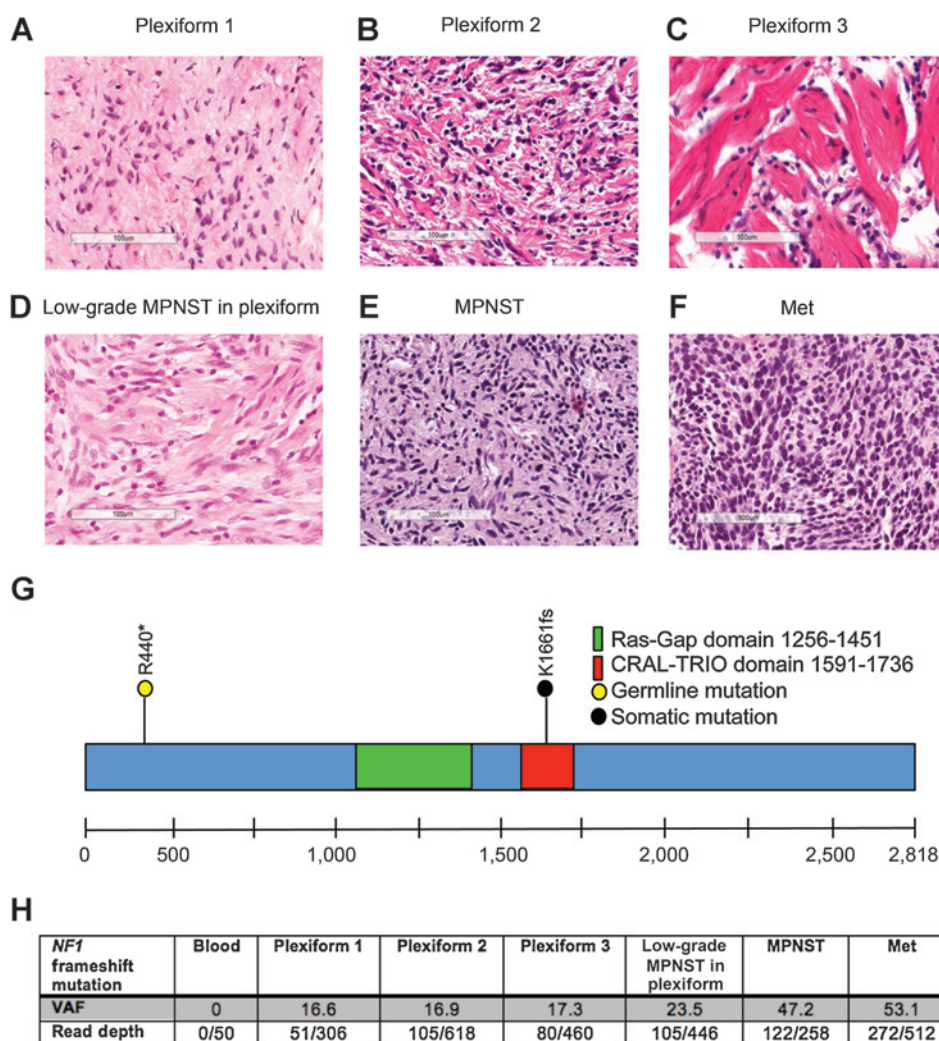


Figure 1. Identification of the germline *NF1* gene mutation in the discovery patient and the somatic *NF1* gene mutation in tumor samples from this individual. Representative images of the Plexiform 1 (A), Plexiform 2 (B), Plexiform 3 (C), Low-Grade MPNST within Plexiform (D), primary high-grade MPNST (E), and metastatic MPNST (F). All images are at ×20 magnification. Scale bars, 100 µm. Diagram of the *NF1* gene depicting the germline and somatic mutations identified in the discovery patient (G). Variant allele frequencies (VAF) with read depths for the somatic *NF1* gene mutation in each tumor sample from the discovery patient (H).

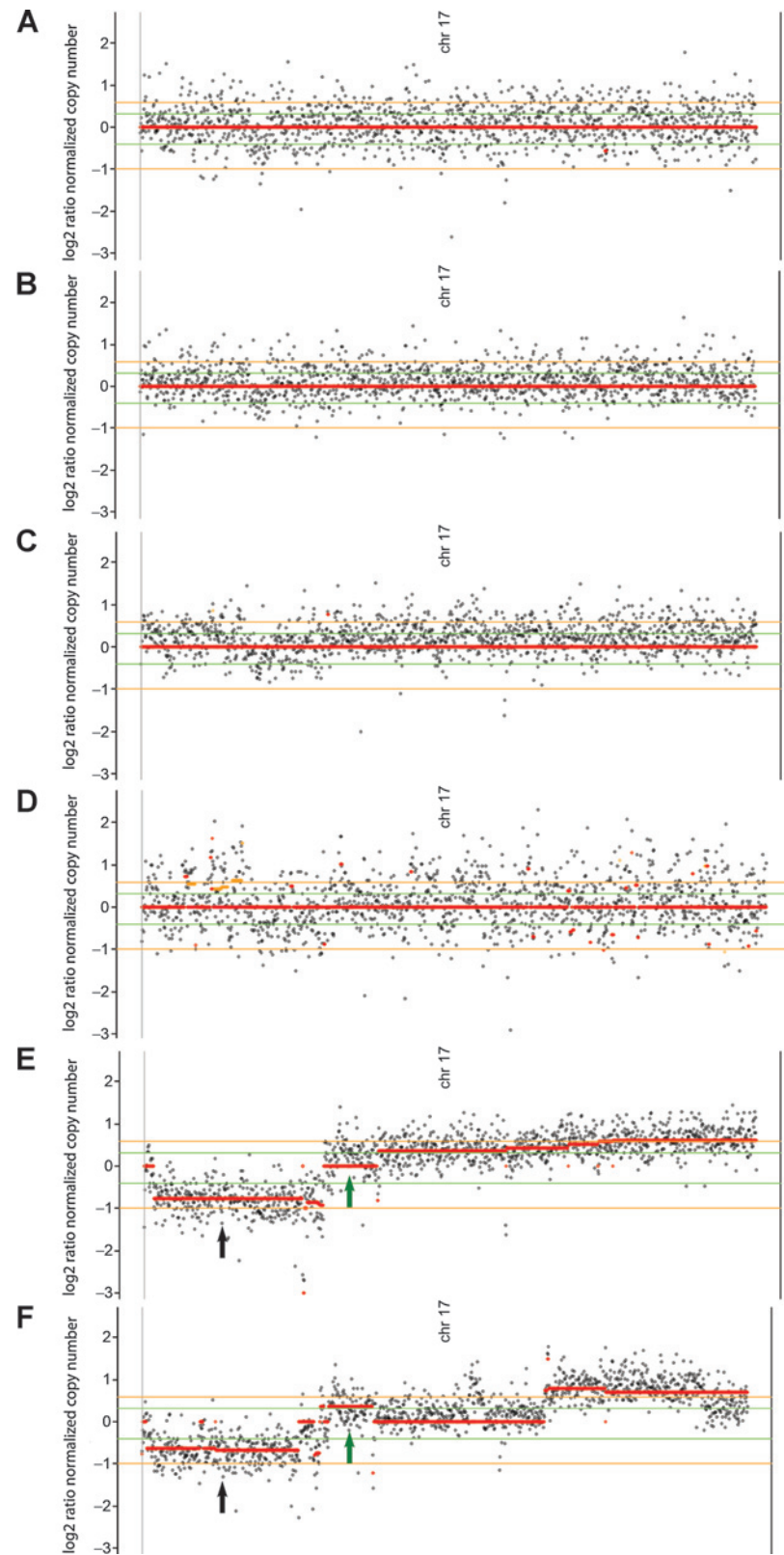
Subcutaneous (s.c.) tumor cell injections

A total of 2×10^5 JW18.2-sh*Sptbn2* or JW18.2-sh*LacZ* tumor cells were injected subcutaneously on the dorsal surface of anesthetized

5-week-old female C57BL6 mice (Taconic) and imaged at days 5, 9, 12, and 16 postinjection ($n = 5$ mice/group). The experiment was repeated independently, and similar results were obtained.

Figure 2.

Copy number plots depicting no alteration at chromosome 17 in Plexiform 1 (A), Plexiform 2 (B), Plexiform 3 (C), and Low-Grade MPNST within Plexiform (D). In contrast, loss of one copy of the area of chromosome 17 encompassing the *TP53* gene was observed in the primary (E) and metastatic (F) MPNST lesions. The area localizing to *TP53* is indicated with a black arrow. The green arrow denotes the area of chromosome 17 amplified in the MPNST and metastatic tumor. The x axis is the \log_2 ratio of the normalized copy number. All samples are normalized to a 0 copy number state. Positive numbers denote amplification, whereas negative numbers denote deletions. Red lines represent areas that the software calls constant copy number variation. Green lines represent one gain or loss in half of the cells. Orange lines represent one gain or loss in all of the cells.



Hirbe et al.

Table 1. Genes mutated in tumors from the index case

| Gene | Blood | Plexiform 1 | Plexiform 2 | Plexiform 3 | Mixed | MPNST | Met | Mutation | Mutation Type | Known Functional Domain |
|---------|-----------|---------------|---------------|---------------|---------------|---------------|----------------|----------|---------------|-------------------------|
| | VAF | VAF | VAF | VAF | Plexiform VAF | VAF | VAF | | | |
| MYB | 0 (0/65) | 15.1 (35/231) | 17.9 (76/421) | 12.0 (35/290) | 18.8 (68/361) | 49.6 (67/135) | 30.0 (91/303) | p.P227L | missense | No |
| SPTBN2 | 0 (0/47) | 0 (0/55) | 0 (0/121) | 0 (0/84) | 0 (0/55) | 62.6 (42/67) | 0 (0/108) | e1-3 | Splice region | No |
| DSCC1 | 0 (0/41) | 0 (0/258) | 0 (0/446) | 0 (0/360) | 0 (0/379) | 31.9 (62/192) | 0 (0/439) | p.I268K | missense | Yes |
| KCNH8 | 0 (0/69) | 0 (0/171) | 0.2 (1/371) | 0.4 (1/236) | 0.6 (2/296) | 46.8 (60/127) | 19.5 (79/404) | p.R418Q | missense | Yes |
| PPFIBP2 | 0 (0/80) | 0 (0/216) | 0.3 (1/329) | 0 (0/243) | 0.4 (1/225) | 28.4 (48/168) | 14.7 (68/460) | p.E301Q | missense | No |
| HEPH | 0 (0/167) | 0.5 (1/194) | 0 (0/311) | 0 (0/258) | 0 (0/192) | 61.9 (65/105) | 64.8 (258/398) | p.F975I | missense | Yes |
| ZNF208 | 0 (0/159) | 0 (0/216) | 0.3 (1/330) | 0 (0/243) | 0.4 (1/226) | 0 (0/108) | 14.8 (68/460) | p.Q25H | missense | Yes |

NOTE: Blue, mutated in all samples. Pink, mutated only in high-grade MPNST. Gray, mutated in high-grade MPNST and metastatic lesion. Purple, mutated only in metastatic lesion.

*VAF = variant allele frequency, read depth follows in parentheses.

Statistical analysis

In vitro and *in vivo* tumor growth data were analyzed on GraphPad Prism Version 5.03. A two-way ANOVA analysis was used to determine statistical significance.

Results and Discussion

Whole-exome sequencing was performed on tumor samples and matched normal blood from one single individual with NF1 followed for over 14 years since childhood by a single physician (D.H. Gutmann) at Washington University. She was initially diagnosed using established clinical criteria (24) as a young child when she presented with multiple café-au-lait macules, skinfold freckling, and a mother with NF1. At age 12, she was initially diagnosed with an enlarging plexiform neurofibroma in her left hemipelvis (Plexiform 1), which was biopsied and demonstrated areas of nuclear pleomorphism worrisome for malignancy, prompting surgical removal for diagnostic reasons. Her plexiform neurofibroma recurred on three separate occasions: later that same year (at age 12), at age 14, and again at age 18 (Plexiform 2, Plexiform 3, and low-grade MPNST within Plexiform). The final plexiform neurofibroma specimen contained a few foci suspicious for low-grade MPNST based on increased cellularity, increased nuclear pleomorphism as well as presence of more than isolated mitosis per high power field. At age 25, she was diagnosed with a high-grade MPNST arising in the same location, which was surgically removed. One year later, at age 26, she developed widely metastatic disease, with lung metastases as well as retroperitoneal involvement. One right-sided retroperitoneal lesion was biopsied (Met), confirming metastatic disease. Histologic sections were evaluated by a pathologist (S.M. Dahiya), and laser capture microdissection was performed to obtain pure tumor samples. Representative images of these tumors are shown in Fig. 1A–F.

Samples were sequenced to achieve a minimum coverage of all targeted space at a minimum of >80% coverage with >20× coverage. In this individual, the germline *NF1* gene mutation was identified (nonsense mutation; R440*), based on its presence in both the blood and tumor specimens (Fig. 1G). In addition, the somatic *NF1* gene mutation was found to be a 4-bp deletion, leading to a frameshift mutation (K1661_fs; Fig. 1G). Using whole-exome sequencing, the mutant *NF1* variant allele frequencies (VAF) were quantified in each of the tumors. An increase in the percentage of tumor cells harboring this somatic *NF1* gene mutation was observed as the tumors evolved from benign plexiform lesions to primary and metastatic MPNST (Fig. 1H). This increase suggests a clonal evolution in the development of this malignancy. Because the DNA was extracted using laser capture microdissection, the samples obtained were relatively devoid of contaminating cells, as evidenced by VAF estimates of approximately 50% in the primary and metastatic MPNST lesions (presence of the somatic *NF1* gene mutation in nearly all tumor cells). These findings are consistent with one prior report in which molecular analysis of a single MPNST divided into benign plexiform neurofibroma, atypical plexiform neurofibroma, and MPNST revealed 9%, 42%, and 97% loss of heterozygosity at the *NF1* locus, respectively (38).

Next, we evaluated the possibility that large-scale somatic rearrangements in other genes cooperate with *NF1* gene loss during the development of MPNSTs. Using copy number alteration analysis of whole-exome read data, few copy number alterations were detected in the benign precursor lesions. In striking contrast, a number of copy number alterations were observed in the primary and metastatic MPNST lesions (Supplementary Fig. S2 and Supplementary Table S2). Although some of these alterations have been observed in other studies (Supplementary Table S3; refs. 16, 39–42), most of these copy number alterations were found only in the primary MPNST from the discovery patient. Moreover,

Table 2. Percentage of mutations in each gene by cancer subtype from the cancer genome atlas database, last updated June 2014 (55, 56)

| Gene | GBM | Mel | NSCL | SCL | Ovary | Uterine | Bladder | Cervical | Gastric | CRC | Breast | Sarc | AML | Head/Neck | Panc | RCC | Liver | Prost | Thy |
|---------|------|------|------|------|-------|---------|---------|----------|---------|-----|--------|------|-----|-----------|------|-----|-------|-------|-----|
| MYB | 1.7 | 5.3 | 2.5 | 10.3 | 2.3 | 3.6 | 7.7 | 0 | 4.1 | 1.4 | 3.7 | 4.7 | 1.1 | 1.4 | 0 | 1 | 1 | 0.4 | 0 |
| SPTBN2 | 0.4 | 10.7 | 6.3 | 3.4 | 4.2 | 10.4 | 7.1 | 5.6 | 9.1 | 4.7 | 4.8 | 1.3 | 0.5 | 10.8 | 0 | 1 | 3 | 2 | 0 |
| DSCC1 | 1.7 | 4.6 | 7 | 3.4 | 34.4 | 4.6 | 8.7 | 5.6 | 9.6 | 5 | 18.8 | 7.3 | 0.5 | 8.3 | 8.2 | 1.2 | 18.1 | 5.3 | 0.3 |
| KCNH8 | 1.7 | 7.6 | 6.8 | 6.9 | 2.9 | 5 | 9.4 | 0 | 8.7 | 4.1 | 2.5 | 2 | 0.5 | 2.2 | 0 | 4.1 | 0.5 | 0.8 | 0 |
| PPFIBP2 | 1.1 | 2.3 | 1.4 | 2.4 | 1 | 4.6 | 3.8 | 0 | 1.4 | 1.8 | 1.6 | 1.3 | 0 | 1.1 | 2 | 0.5 | 0.5 | 0.8 | 0 |
| HEPH | 0.7 | 10.3 | 7.7 | 10.3 | 5.1 | 9.2 | 2.4 | 0 | 5.9 | 2.3 | 2.4 | 7.3 | 0.5 | 4.3 | 2 | 0.5 | 0.5 | 29.5 | 0 |
| ZNF208 | 2.1 | 14.1 | 12.7 | 11.9 | 7 | 9.2 | 7.9 | 2.8 | 11 | 5.7 | 3 | 3.3 | 0 | 7.3 | 4.1 | 0.5 | 2.5 | 2 | 0 |
| NF1 | 17.6 | 14.1 | 12 | 2.4 | 11.9 | 11.3 | 11 | 8.3 | 6.8 | 5.2 | 5.4 | 3.3 | 2.7 | 3.3 | 2 | 1.7 | 1.5 | 1.2 | 0.8 |

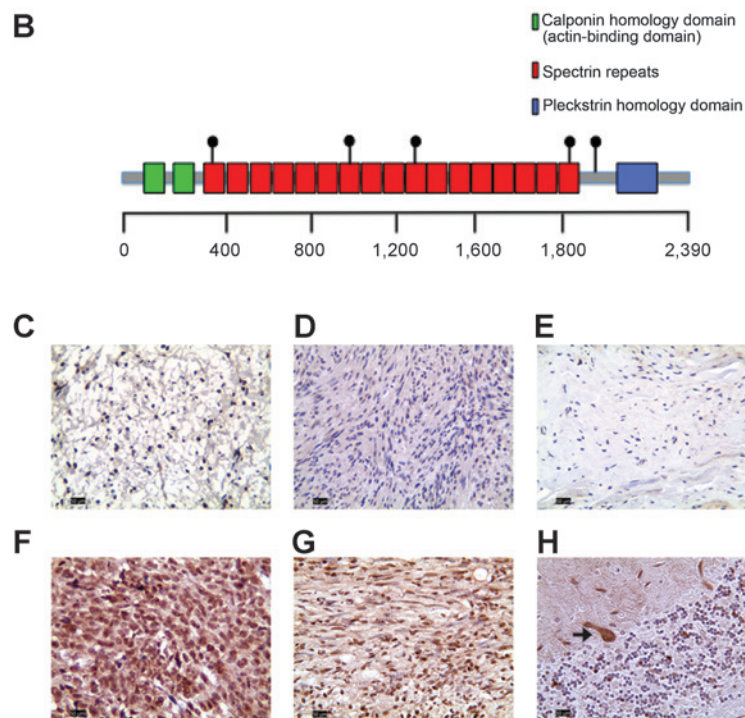
Abbreviations: GBM, glioblastoma multiforme; Mel, melanoma; NSCLC, non-small cell lung cancer; SCL, small cell lung; CRC, colorectal cancer; Sarc, sarcoma; AML, acute myeloid leukemia; Panc, pancreas; RCC, renal cell cancer; Prost, prostate; Thy, thyroid.

A

| Gene | Mutations in plexiform | Mutations in MPNST | Mutations in metastases |
|----------------|------------------------|--------------------|-------------------------|
| <i>MYB</i> | 0/6 | 0 | 0/5 |
| <i>SPTBN2</i> | 0/6 | 4/15 | 1/5 |
| <i>DSCC1</i> | 0/6 | 1/15 | 0/5 |
| <i>KCNH8</i> | 0/6 | 1/15 | 0/5 |
| <i>PPFIBP2</i> | 0/6 | 2/15 | 0/5 |
| <i>HEPH</i> | 0/6 | 2/15 | 0/5 |
| <i>ZNF208</i> | 0/6 | 0/15 | 1/5 |

Figure 3.

Genes mutated in the MPNST validation set (A). A schematic representation of the β_{III} -spectrin protein with the location of the missense mutations denoted. Mutations were also identified in the splice region predicting exon skipping and in the 5' untranslated region (not pictured). Positive β_{III} -spectrin immunostaining was not found in neurofibromas (C), schwannomas (D), or normal peripheral nerve (E), but was observed in the majority of MPNSTs with *SPTBN2* mutations (F) as well as in MPNSTs without *SPTBN2* mutations (G). H, normal cerebellum was included as an internal control for positive β_{III} -spectrin immunostaining. Arrow denotes the β_{III} -spectrin-immunoreactive Purkinje cells.



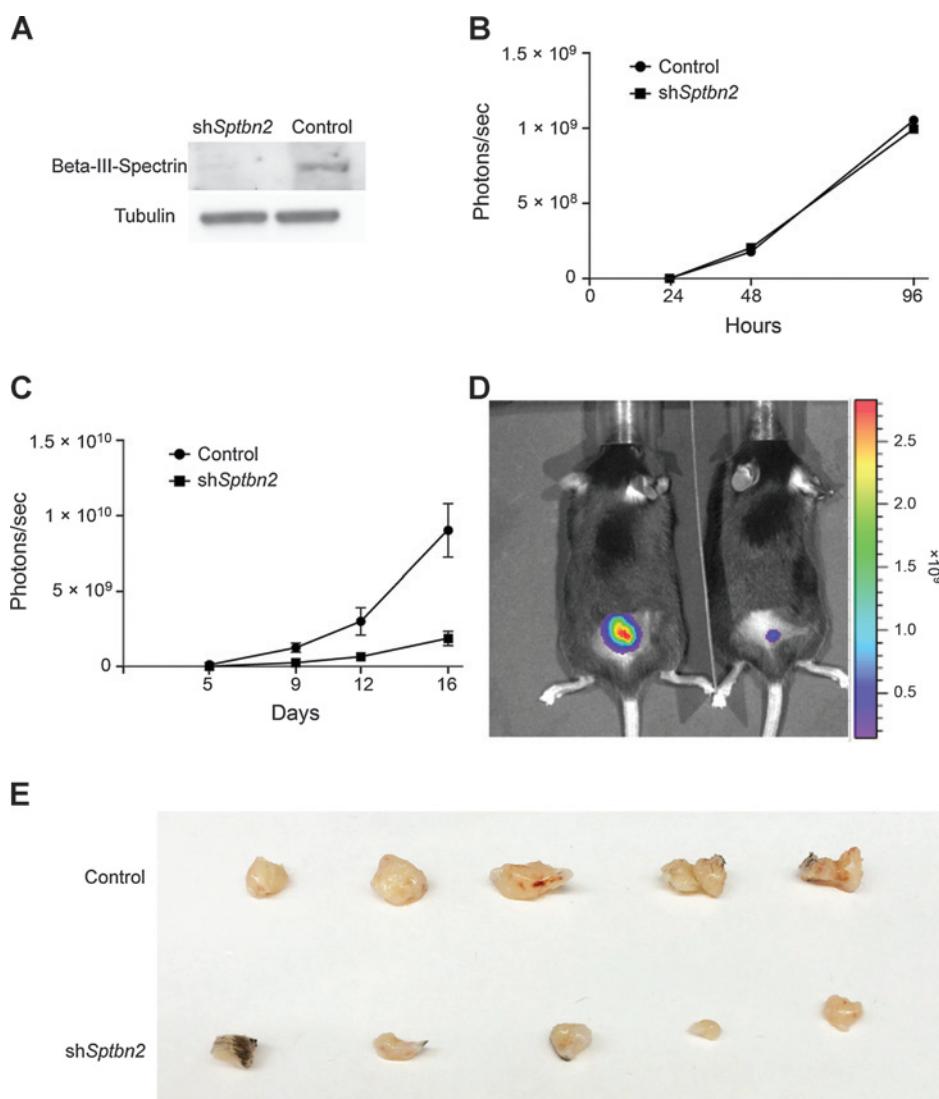
some of these alterations were only observed in the primary MPNST and not in the metastatic tumor (*SPTBN2* and *DSCC1*).

To identify areas of overlap shared between the primary and metastatic MPNST, a high confidence event identified involved loss of an area of chromosome 17p containing the *TP53* tumor suppressor gene (Fig. 2). Previous studies also support a causative role for loss of p53 function during malignant progression to MPNST (43). In further support of this notion, 30% to 50% of genetically engineered mice heterozygous for germline *Nf1* and *Tp53* mutations develop MPNSTs (44, 45). However in people, *TP53* haploinsufficiency, rather than bi-allelic *TP53* inactivation, may be sufficient for MPNST development (46, 47). As such, bi-allelic *TP53* loss was only observed in 3 of 14 MPNSTs (46). It is also possible that other cell-cycle regulators (e.g., p16) are inactivated in cases where bi-allelic *TP53* mutations are not observed; however, *CDKN2A* deletions were not observed in our patient, as reported in some other studies (21, 48–50). Interestingly, there was an area on chromosome 17 amplified in both the MPNST and metastatic lesion containing the *BIRC5* and *SOX9* genes (Fig. 2), both of which have been previously found in MPNSTs (17, 40, 51,

52). Although *BIRC5* and *SOX9* are involved in cell survival (53, 54), their role in MPNST pathogenesis remains to be defined.

In addition to *TP53* loss, 42 somatic variants (including missense, nonsense, splice site, deletions, insertions, and silent mutations) were identified (Supplementary Table S4). Of these somatic variants, mutations found only in the benign tumors, silent mutations, and those resulting in conservative amino acid changes were excluded from further study. Following this filtering, nine genes were selected for resequencing at a greater read depth (>40 \times coverage) and after manual review, only seven genes remained (Table 1). Mutations in these seven genes have previously been reported in various malignancies in the cancer genome atlas (TCGA) database (Table 2; refs. 55, 56), underscoring their potential significance in tumorigenesis. Interestingly, we did not observe *EGFR* amplification in this specific MPNST case, as previously reported for other MPNSTs (21). Similarly, no copy number gains were identified involving chromosomes 12p12.1, 12p13.31, 12p13.33, or 12q14.1 (16). These results raise the intriguing possibility that there are multiple molecular routes to MPNST.

Hirbe et al.

**Figure 4.**

β_{III} -spectrin knockdown attenuates MPNST growth *in vivo*. A, Western blotting reveals decreased β_{III} -spectrin expression in shSptbn2-infected JW18.2 cells relative to control shLacZ-infected cells. α -tubulin was included as an internal protein loading control. B, *in vitro* cell proliferation was assessed by BLI at 24, 48, and 96 hours post-plating ($P = 0.276$). C, *in vivo* tumor growth was assessed by BLI at 5, 9, 12, and 16 days postinjection. Photon flux was quantitated in a fixed region of interest (ROI) over the subcutaneously implanted tumor ($P < 0.001$; $n = 5$ mice/group). D, representative images of mice injected with shSptbn2-infected cells relative to those injected with control shLacZ-infected cells are shown. E, gross images of the dissected tumors are shown.

To determine whether these seven genes are mutated in other individuals with NF1-MPNST, directed sequencing was performed in six plexiform neurofibromas, fifteen primary MPNSTs, and five metastatic MPNSTs. While none of these genes were mutated in the plexiform neurofibroma tumors, 5 of the 7 genes were mutated in these independently identified MPNSTs (Fig. 3A). ZNF208 was the only gene uniquely mutated in the metastatic MPNST specimen (Table 1; Fig. 3A and Supplementary Table S5). ZNF208 is a member of a large family of zinc finger proteins containing Kruppel-associated box domains, which serve as transcriptional regulators (57). Unfortunately, there is a paucity of information about ZNF208 function in mammalian cells. It is worth noting that ZNF208 protein expression was detected by IHC in the metastatic tumor in this study as well as in one additional metastatic MPNST (data not shown). The lack of additional matched MPNST/metastatic lesion specimens with sufficient tissue for analysis precluded a more extensive analysis.

The most frequently mutated gene was the SPTBN2 gene encoding β_{III} -spectrin, a cytoskeletal protein (Fig. 3A and Supplementary Table S5). Different types of mutations were observed, including missense mutations ($n = 5$), silent mutations

($n = 3$), one mutation predicted to cause exon-skipping, and one mutation in the 5-prime untranslated region (Fig. 3B). In addition, one MPNST harbored several different mutations within the SPTBN2 gene. Given that this gene was the most frequently mutated gene in the MPNSTs examined (5/16 tumors), albeit at low variant allele frequencies, we next sought to determine whether deregulated β_{III} -spectrin expression was observed in these cancers. Robust β_{III} -spectrin immunoreactivity was found in all MPNSTs in the validation set (15/15) regardless of mutational status (Fig. 3F and G). Similarly, examination of additional MPNSTs, both sporadic and NF1-associated, from two previously generated tissue microarray revealed strong β_{III} -spectrin immunoreactivity in nearly all MPNSTs (45/50 tumors; 90% samples). In striking contrast, β_{III} -spectrin immunoreactivity was not observed in benign neurofibromas (0/4), schwannomas (0/4), or normal peripheral nerve (0/2; Fig. 3C–E).

Spectrins are cytoskeletal, heterodimeric proteins composed of α - and β subunits, with important roles in maintaining the stability of the cell membrane, promoting adhesion and spreading, regulating Golgi and vesicular transport, and controlling cell-cycle progression (58–61). Moreover, β_{III} -spectrin can enhance

cell survival through maintenance of the Golgi apparatus and regulation of cell surface receptor vesicular transport, including glutamate receptors (60–62). In addition, a related spectrin molecule (β_{III} -spectrin; fodrin) interacts with the protein product (merlin/schwannomin) mutated in the Neurofibromatosis type II (NF2) Schwann cell cancer predisposition syndrome (63). On the basis of these observations, we speculate that the observed *SPTBN2* mutations represent gain-of-function alterations.

To assess the potential functional significance of the increased β_{III} -spectrin found in the majority of human MPNSTs, we examined β_{III} -spectrin protein expression by IHC in four *Nf1/Trp53*-mutant NPcis MPNST cell lines engineered to express luciferase. Interestingly, the MPNST cell line with the greatest β_{III} -spectrin expression exhibited the fastest growth rate following subcutaneous transplantation into immunocompetent mice by bioluminescence imaging *in vivo* (JW18.2; data not shown). For this reason, JW18.2 was chosen for further study. Following *Sptbn2* shRNA-mediated knockdown, there was reduced β_{III} -spectrin expression by Western blot analysis relative to control shLacZ virus infection (Fig. 4A). No difference in cell growth was observed following β_{III} -spectrin knockdown *in vitro*, as measured by BLI at 24, 48, and 96 hours (Fig. 4B) or direct cell counting (data not shown). However, β_{III} -spectrin knockdown attenuated tumor growth *in vivo* (Fig. 4C–E), supporting a role for this spectrin family member in MPNST maintenance. Collectively, these *in vivo* results coupled with the observation that MPNSTs harbor a high frequency of *SPTBN2* mutation and β_{III} -spectrin immunoreactivity should prompt further mechanistic investigation into the role of this new MPNST-associated gene in cancer pathogenesis.

In summary, this study represents the first use of whole-exome sequencing to capture the molecular events that accompany the progression of a benign plexiform neurofibroma to malignancy and metastasis in a single individual. Although the sequence and nature of genetic alterations might be specific to a given individual, the discovery of β_{III} -spectrin as a frequently mutated gene and overexpressed protein in other MPNSTs underscores the value of this approach in identifying new targets for future study.

References

- Arun D, Gutmann DH. Recent advances in neurofibromatosis type 1. *Curr Opin Neurol* 2004;17:101–5.
- Hirbe AC, Gutmann DH. Neurofibromatosis type 1: a multidisciplinary approach to care. *Lancet Neurol* 2014;13:834–43.
- Ferner RE, Huson SM, Thomas N, Moss C, Willshaw H, Evans DG, et al. Guidelines for the diagnosis and management of individuals with neurofibromatosis 1. *J Med Genet* 2007;44:81–8.
- Upadhyaya M, Spurlock G, Monem B, Thomas N, Friedrich RE, Kluwe L, et al. Germline and somatic NF1 gene mutations in plexiform neurofibromas. *Hum Mutat* 2008;29:E103–11.
- Rasmussen SA, Overman J, Thomson SA, Colman SD, Abernathy CR, Trimpert RE, et al. Chromosome 17 loss-of-heterozygosity studies in benign and malignant tumors in neurofibromatosis type 1. *Genes Chromosomes Cancer* 2000;28:425–31.
- Perry A, Roth KA, Banerjee R, Fuller CE, Gutmann DH. NF1 deletions in S-100 protein-positive and negative cells of sporadic and neurofibromatosis 1 (NF1)-associated plexiform neurofibromas and malignant peripheral nerve sheath tumors. *Am J Pathol* 2001;159:57–61.
- Reuss DE, Habel A, Hagenlocher C, Mucha J, Ackermann U, Tessmer C, et al. Neurofibromin specific antibody differentiates malignant peripheral nerve sheath tumors (MPNST) from other spindle cell neoplasms. *Acta Neuropathol* 2014;127:565–72.
- Bottillo I, Ahlquist T, Brekke H, Danielsen SA, van den Berg E, Mertens F, et al. Germline and somatic NF1 mutations in sporadic and NF1-

Disclosure of Potential Conflicts of Interest

D.H. Gutmann is listed as an inventor on a patent on NF1 genes, which is owned by The University of Michigan, and mTOR, which is owned by Washington University. No potential conflicts of interest were disclosed by the other authors.

Authors' Contributions

Conception and design: A.C. Hirbe, R.S. Fulton, D.H. Gutmann
Development of methodology: A.C. Hirbe, R.S. Fulton, X. Zhang
Acquisition of data (provided animals, acquired and managed patients, provided facilities, etc.): A.C. Hirbe, R.S. Fulton, S. McDonald, J. Walrath, K.M. Reilly, M. Pekmezci, A. Perry, S. Dahiya, K. DeSchryver
Analysis and interpretation of data (e.g., statistical analysis, biostatistics, computational analysis): A.C. Hirbe, C.A. Miller, T. Li, R.S. Fulton, E.J. Duncavage, H.J. Abel, D.H. Gutmann
Writing review, and/or revision of the manuscript: A.C. Hirbe, T. Li, R.S. Fulton, S. McDonald, E.J. Duncavage, M. Pekmezci, A. Perry, D.H. Gutmann, S. Dahiya, K. DeSchryver
Administrative, technical, or material support (i.e., reporting or organizing data, constructing databases): X. Zhang, D.H. Gutmann
Study supervision: T.J. Ley
Other (manage tissue sample, perform LCM and DNA isolation): X. Zhang

Acknowledgments

The authors thank Drs. Brian A. Van Tine and Anthony J. Apicelli for helpful discussions, Scott Gianino, Tyler Smallman, and Julie Prior for technical assistance, and Heather Schmidt for manual review of predicted mutations.

Grant Support

This work was partly funded by a generous gift from Schnuck Markets Inc. (to D.H. Gutmann). A.C. Hirbe was supported on the T32 HL007088. BLI was performed at the Washington University Molecular Imaging Center, supported by NIH P50 CA094056. Lentivirus was generated by the Washington University Hope Center Viral Vectors Core, which is supported by a Neuroscience Blueprint Core grant NIH P30 NS057105.

The costs of publication of this article were defrayed in part by the payment of page charges. This article must therefore be hereby marked *advertisement* in accordance with 18 U.S.C. Section 1734 solely to indicate this fact.

Received November 26, 2014; revised March 23, 2015; accepted April 14, 2015; published OnlineFirst April 29, 2015.

- associated malignant peripheral nerve sheath tumours. *J Pathol* 2009; 217:693–701.
- Yang FC, Ingram DA, Chen S, Zhu Y, Yuan J, Li X, et al. Nf1-dependent tumors require a microenvironment containing Nf1 +/- and c-kit-dependent bone marrow. *Cell* 2008;135:437–48.
- Zheng H, Chang L, Patel N, Yang J, Lowe L, Burns DK, et al. Induction of abnormal proliferation by nonmyelinating schwann cells triggers neurofibroma formation. *Cancer Cell* 2008;13:117–28.
- Zhu Y, Ghosh P, Charnay P, Burns DK, Parada LF. Neurofibromas in NF1: Schwann cell origin and role of tumor environment. *Science* 2002;296: 920–2.
- Wu J, Williams JP, Rizvi TA, Kordich JJ, Witte D, Meijer D, et al. Plexiform and dermal neurofibromas and pigmentation are caused by Nf1 loss in desert hedgehog-expressing cells. *Cancer Cell* 2008;13:105–16.
- Brossier NM, Carroll SL. Genetically engineered mouse models shed new light on the pathogenesis of neurofibromatosis type 1-related neoplasms of the peripheral nervous system. *Brain Res Bull* 2012;88:58–71.
- Watson MA, Perry A, Tihan T, Prayson RA, Guha A, Bridge J, et al. Gene expression profiling reveals unique molecular subtypes of Neurofibromatosis Type 1-associated and sporadic malignant peripheral nerve sheath tumors. *Brain Pathol* 2004;14:297–303.
- Riddle ND, Gorden L, Rojiani MV, Hakam A, Rojiani AM. CD44 and p53 immunopositive patterns in NF1 neoplasms - indicators of malignancy and infiltration. *Int J Clin Exp Pathol* 2010;3:515–21.

Hirbe et al.

16. Yu J, Deshmukh H, Payton JE, Dunham C, Scheithauer BW, Tihan T, et al. Array-based comparative genomic hybridization identifies CDK4 and FOXM1 alterations as independent predictors of survival in malignant peripheral nerve sheath tumor. *Clin Cancer Res* 2011;17:1924–34.
17. Miller SJ, Jessen WJ, Mehta T, Hardiman A, Sites E, Kaiser S, et al. Integrative genomic analyses of neurofibromatosis tumours identify SOX9 as a biomarker and survival gene. *EMBO Mol Med* 2009;1:236–48.
18. Upadhyaya M, Spurlock G, Thomas L, Thomas NS, Richards M, Mautner VF, et al. Microarray-based copy number analysis of neurofibromatosis type-1 (NF1)-associated malignant peripheral nerve sheath tumors reveals a role for Rho-GTPase pathway genes in NF1 tumorigenesis. *Hum Mutat* 2012;33:763–76.
19. Danielsen SA, Lind GE, Kolberg M, Holand M, Bjerkehagen B, Sundby Hall K, et al. Methylated RASSF1A in malignant peripheral nerve sheath tumors identifies neurofibromatosis type 1 patients with inferior prognosis. *Neuro Oncol* 2015;17:63–9.
20. Park GH, Lee SJ, Yim H, Han JH, Kim HJ, Sohn YB, et al. TAGLN expression is upregulated in NF1-associated malignant peripheral nerve sheath tumors by hypomethylation in its promoter and subpromoter regions. *Oncol Rep* 2014;32:1347–54.
21. Perry A, Kunz SN, Fuller CE, Banerjee R, Marley EF, Liapis H, et al. Differential NF1, p16, and EGFR patterns by interphase cytogenetics (FISH) in malignant peripheral nerve sheath tumor (MPNST) and morphologically similar spindle cell neoplasms. *J Neuropathol Exp Neurol* 2002;61:702–9.
22. Holtkamp N, Mautner VF, Friedrich RE, Harder A, Hartmann C, Theallier-Janko A, et al. Differentially expressed genes in neurofibromatosis 1-associated neurofibromas and malignant peripheral nerve sheath tumors. *Acta Neuropathol* 2004;107:159–68.
23. Fang Y, Elahi A, Denley RC, Rao PH, Brennan MF, Jhanwar SC. Molecular characterization of permanent cell lines from primary, metastatic and recurrent malignant peripheral nerve sheath tumors (MPNST) with underlying neurofibromatosis-1. *Anticancer Res* 2009;29:1255–62.
24. National Institutes of Health Consensus Development Conference Statement: neurofibromatosis. Bethesda, Md., USA, July 13–15, 1987. *Neurofibromatosis* 1988;1:172–8.
25. Li H, Durbin R. Fast and accurate short read alignment with Burrows-Wheeler transform. *Bioinformatics* 2009;25:1754–60.
26. Li H, Handsaker B, Wysoker A, Fennell T, Ruan J, Homer N, et al. The Sequence Alignment/Map format and SAMtools. *Bioinformatics* 2009;25:2078–9.
27. Larson DE, Harris CC, Chen K, Koboldt DC, Abbott TE, Dooling DJ, et al. SomaticSniper: identification of somatic point mutations in whole genome sequencing data. *Bioinformatics* 2012;28:311–7.
28. Koboldt DC, Zhang Q, Larson DE, Shen D, McLellan MD, Lin L, et al. VarScan 2: somatic mutation and copy number alteration discovery in cancer by exome sequencing. *Genome Res* 2012;22:568–76.
29. Saunders CT, Wong WS, Swamy S, Becq J, Murray LJ, Cheetham RK, Strelka: accurate somatic small-variant calling from sequenced tumor-normal sample pairs. *Bioinformatics* 2012;28:1811–7.
30. McKenna A, Hanna M, Banks E, Sivachenko A, Cibulskis K, Kernysky A, et al. The Genome Analysis Toolkit: a MapReduce framework for analyzing next-generation DNA sequencing data. *Genome Res* 2010;20:1297–303.
31. Ye K, Schulz MH, Long Q, Apweiler R, Ning Z. Pindel: a pattern growth approach to detect break points of large deletions and medium sized insertions from paired-end short reads. *Bioinformatics* 2009;25:2865–71.
32. Hirbe AC, Pekmezci M, Dahiya S, Apicelli AJ, Van Tine BA, Perry A, et al. BRAFV600E mutation in sporadic and neurofibromatosis type 1-related malignant peripheral nerve sheath tumors. *Neuro Oncol* 2014;16:466–7.
33. Uhlmann EJ, Li W, Scheidenhelm DK, Gau CL, Tamanoi F, Gutmann DH. Loss of tuberous sclerosis complex 1 (Tsc1) expression results in increased Rheb/S6K pathway signaling important for astrocyte cell size regulation. *Glia* 2004;47:180–8.
34. Turbyville TJ, Gursel DB, Tuskan RG, Walrath JC, Lipschultz CA, Lockett SJ, et al. Schweinfurthin A selectively inhibits proliferation and Rho signaling in glioma and neurofibromatosis type 1 tumor cells in a NF1-GRD-dependent manner. *Mol Cancer Ther* 2010;9:1234–43.
35. Reilly KM, Loisel DA, Bronson RT, McLaughlin ME, Jacks T. Nf1/Trp53 mutant mice develop glioblastoma with evidence of strain-specific effects. *Nat Genet* 2000;26:109–13.
36. Smith MC, Luker KE, Garbow JR, Prior JL, Jackson E, Piwnica-Worms D, et al. CXCR4 regulates growth of both primary and metastatic breast cancer. *Cancer Res* 2004;64:8604–12.
37. Warrington NM, Gianino SM, Jackson E, Goldhoff P, Garbow JR, Piwnica-Worms D, et al. Cyclic AMP suppression is sufficient to induce gliomagenesis in a mouse model of neurofibromatosis-1. *Cancer Res* 2010;70:5717–27.
38. Spurlock G, Knight SJ, Thomas N, Kiehl TR, Guha A, Upadhyaya M. Molecular evolution of a neurofibroma to malignant peripheral nerve sheath tumor (MPNST) in an NF1 patient: correlation between histopathological, clinical and molecular findings. *J Cancer Res Clin Oncol* 2010;136:1869–80.
39. Mantripragada KK, Spurlock G, Kluge L, Chuzhanova N, Ferner RE, Frayling IM, et al. High-resolution DNA copy number profiling of malignant peripheral nerve sheath tumors using targeted microarray-based comparative genomic hybridization. *Clin Cancer Res* 2008;14:1015–24.
40. Miller SJ, Rangwala F, Williams J, Ackerman P, Kong S, Jegga AG, et al. Large-scale molecular comparison of human schwann cells to malignant peripheral nerve sheath tumor cell lines and tissues. *Cancer Res* 2006;66:2584–91.
41. Levy P, Vidaud D, Leroy K, Laurendeau I, Wechsler J, Bolasco G, et al. Molecular profiling of malignant peripheral nerve sheath tumors associated with neurofibromatosis type 1, based on large-scale real-time RT-PCR. *Mol Cancer* 2004;3:20.
42. Skotheim RI, Kallioniemi A, Bjerkehagen B, Mertens F, Brekke HR, Monni O, et al. Topoisomerase-II alpha is upregulated in malignant peripheral nerve sheath tumors and associated with clinical outcome. *J Clin Oncol* 2003;21:4586–91.
43. Legius E, Dierick H, Wu R, Hall BK, Marynen P, Cassiman JJ, et al. TP53 mutations are frequent in malignant NF1 tumors. *Genes Chromosomes Cancer* 1994;10:250–5.
44. Cichowski K, Shih TS, Schmitt E, Santiago S, Reilly K, McLaughlin ME, et al. Mouse models of tumor development in neurofibromatosis type 1. *Science* 1999;286:2172–6.
45. Vogel KS, Klesse LJ, Velasco-Miguel S, Meyers K, Rushing EJ, Parada LF. Mouse tumor model for neurofibromatosis type 1. *Science* 1999;286:2176–9.
46. Lothe RA, Smith-Sorensen B, Hektoen M, Stenwig AE, Mandahl N, Saeter G, et al. Biallelic inactivation of TP53 rarely contributes to the development of malignant peripheral nerve sheath tumors. *Genes Chromosomes Cancer* 2001;30:202–6.
47. Rahrmann EP, Moriarity BS, Otto GM, Watson AL, Choi K, Collins MH, et al. Trp53 haploinsufficiency modifies EGFR-driven peripheral nerve sheath tumorigenesis. *Am J Pathol* 2014;184:2082–98.
48. Nielsen GP, Stemmer-Rachamimov AO, Ino Y, Moller MB, Rosenberg AE, Louis DN. Malignant transformation of neurofibromas in neurofibromatosis 1 is associated with CDKN2A/p16 inactivation. *Am J Pathol* 1999;155:1879–84.
49. Perrone F, Tabano S, Colombo F, Dagrada G, Birindelli S, Gronchi A, et al. p15INK4b, p14ARF, and p16INK4a inactivation in sporadic and neurofibromatosis type 1-related malignant peripheral nerve sheath tumors. *Clin Cancer Res* 2003;9:4132–8.
50. Beert E, Brems H, Daniels B, De Wever I, Van Calenbergh F, Schoenaers J, et al. Atypical neurofibromas in neurofibromatosis type 1 are premalignant tumors. *Genes Chromosomes Cancer* 2011;50:1021–32.
51. Storlazzi CT, Brekke HR, Mandahl N, Brosjo O, Smeland S, Lothe RA, et al. Identification of a novel amplicon at distal 17q containing the BIRC5/SURVIVIN gene in malignant peripheral nerve sheath tumours. *J Pathol* 2006;209:492–500.
52. Alaggio R, Turrini R, Boldrin D, Merlo A, Gambini C, Ferrari A, et al. Survivin expression and prognostic significance in pediatric malignant peripheral nerve sheath tumors (MPNST). *PLoS One* 2013;8:e80456.

53. Athanasoula K, Gogas H, Polonifi K, Vaiopoulos AG, Polyzos A, Mantzourani M. Survivin beyond physiology: orchestration of multistep carcinogenesis and therapeutic potentials. *Cancer Lett* 2014;347:175–82.
54. Kolettas E, Muir HI, Barrett JC, Hardingham TE. Chondrocyte phenotype and cell survival are regulated by culture conditions and by specific cytokines through the expression of Sox-9 transcription factor. *Rheumatology* 2001;40:1146–56.
55. Cerami E, Gao J, Dogrusoz U, Gross BE, Sumer SO, Aksoy BA, et al. The cBio cancer genomics portal: an open platform for exploring multidimensional cancer genomics data. *Cancer Discov* 2012;2:401–4.
56. Gao J, Aksoy BA, Dogrusoz U, Dresdner G, Gross B, Sumer SO, et al. Integrative analysis of complex cancer genomics and clinical profiles using the cBioPortal. *Sci Signal* 2013;6:pl1.
57. Lupo A, Cesaro E, Montano G, Zurlo D, Izzo P, Costanzo P. KRAB-Zinc finger proteins: a repressor family displaying multiple biological functions. *Curr Genomics* 2013;14:268–78.
58. Zhang R, Zhang C, Zhao Q, Li D. Spectrin: structure, function and disease. *Sci China Life Sci* 2013;56:1076–85.
59. Armbrust KR, Wang X, Hathorn TJ, Cramer SW, Chen G, Zu T, et al. Mutant beta-III spectrin causes mGluR1alpha mislocalization and functional deficits in a mouse model of spinocerebellar ataxia type 5. *J Neurosci* 2014;34:9891–904.
60. Salcedo-Sicilia L, Granell S, Jovic M, Sicart A, Mato E, Johannes L, et al. betaIII spectrin regulates the structural integrity and the secretory protein transport of the Golgi complex. *J Biol Chem* 2013;288:2157–66.
61. Stankewich MC, Tse WT, Peters LL, Ch'ng Y, John KM, Stabach PR, et al. A widely expressed betaIII spectrin associated with Golgi and cytoplasmic vesicles. *Proc Natl Acad Sci U S A* 1998;95:14158–63.
62. Perkins EM, Clarkson YL, Sabatier N, Longhurst DM, Millward CP, Jack J, et al. Loss of beta-III spectrin leads to Purkinje cell dysfunction recapitulating the behavior and neuropathology of spinocerebellar ataxia type 5 in humans. *J Neurosci* 2010;30:4857–67.
63. Scoles DR, Huynh DP, Morcos PA, Coulsell ER, Robinson NG, Tamanoi F, et al. Neurofibromatosis 2 tumour suppressor schwannomin interacts with betaII-spectrin. *Nat Genet* 1998;18:354–9.

Clinical Cancer Research

Whole Exome Sequencing Reveals the Order of Genetic Changes during Malignant Transformation and Metastasis in a Single Patient with NF1-plexiform Neurofibroma

Angela C. Hirbe, Sonika Dahiya, Christopher A. Miller, et al.

Clin Cancer Res 2015;21:4201-4211. Published OnlineFirst April 29, 2015.

Updated version Access the most recent version of this article at:
doi:[10.1158/1078-0432.CCR-14-3049](https://doi.org/10.1158/1078-0432.CCR-14-3049)

Supplementary Material Access the most recent supplemental material at:
<http://clincancerres.aacrjournals.org/content/suppl/2015/04/29/1078-0432.CCR-14-3049.DC1.html>

Cited articles This article cites 63 articles, 30 of which you can access for free at:
<http://clincancerres.aacrjournals.org/content/21/18/4201.full.html#ref-list-1>

E-mail alerts [Sign up to receive free email-alerts](#) related to this article or journal.

Reprints and Subscriptions To order reprints of this article or to subscribe to the journal, contact the AACR Publications Department at pubs@aacr.org.

Permissions To request permission to re-use all or part of this article, contact the AACR Publications Department at permissions@aacr.org.